Title

Finite-Element Analysis of the Strain Distribution Due to Bending in a REBCO Coated Conductor for Canted Cosine Theta Dipole Magnet Applications

Journal

IEEE Transactions on Applied Superconductivity, 29(5)

ISSN

1051-8223

Authors

Pierro, Federica

Zhao, Zijia

Owen, Casey M

et al.

Publication Date

2019

DOI

10.1109/tasc.2019.2897708

Peer reviewed

Finite element analysis of the strain distribution due to bending in a REBCO coated conductor for Canted Cosine Theta dipole magnet applications

F. Pierro, Z. Zhao, C. M. Owen, C. Colcord, L. Chiesa, H. C. Higley, X. Wang, S. O. Prestemon

***Abstract*—High-current cables using REBCO tapes can be used to develop high-field dipole magnets. However, the strain accumulated during cable fabrication and coil winding may reduce the critical current of the conductor. Therefore, it is important to properly consider the strain when designing high-field magnets. In this work, we used structural finite element analysis to predict the strain experienced by a REBCO tape during bending in configurations relevant to the fabrication of high field accelerator magnets, in particular, the mechanical strain generated during cable fabrication and winding in a canted-cosθ (CCT) dipole configuration.**

We considered two different cable options: (A) flat tape that lay in the mandrel channel and (B) a REBCO tape helically wound around a circular copper core, the typical configuration of the conductor in round core cable (CORC®). Strain accumulated during tape winding is studied for different core diameters and winding tilt angles. FEA longitudinal strain results were compared with the simulations for configuration A, where higher strain was observed experimentally. Configuration B was verified indirectly by comparing experimentally measured *Ic* with the one predicted (based on the longitudinal strain) as function of the bending diameter. Good agreement was found up to a bending diameter of 30 mm. The presented results will help to understand the impact of bending on REBCO tapes and CORC® wires to develop high-field magnets.

***Index Terms*— High-temperature superconductors, yttrium barium copper oxide, superconducting cables, superconducting magnets**

I. Introduction

Future generation particle accelerators will require magnetic fields higher than 20 T [1]. However, reaching such magnetic field using traditional Low Temperature Superconductors (LTS) could be challenging. For NbTi and Nb_3Sn magnet technologies, the maximum achievable dipole magnetic field are respectively 10.5 T and 17-18 T [2]. To achieve higher fields, new magnet technology that utilize High Temperature Superconductors (HTS) needs to be developed. Dipole magnets made with both BSCCO and REBCO conductors have been investigated in the last few years [3]-[8] showing that both conductor choices have challenges. Although REBCO tapes do not require heat treatment, their thin flat geometry makes the cabling difficult. REBCO tapes undergo a bending process during cable fabrication or winding of the coil. The bending affects the critical current (I_c) of the conductor.

The minimum bending diameter (which does not lead to significant I_c degradation) of the conductor is an important parameter in the design of canted-cosθ (CCT) dipole [5] made with REBCO tapes. In this configuration (Fig. 1) the channels have a tilt angle α, and the conductor assumes the shape of an ellipse rather than a circle. As discussed in [6], it is desirable to have small tilt angles to achieve dipole fields more efficiently. However, this will result in small bending diameter at the pole of the ellipse and therefore higher strain on the REBCO conductor and possible current degradation.

The effect of pure bending on specific cables configurations has been studied in [9]-[11]. In [12], a curvature-based analytical model was developed to predict the strain generated in the REBCO layer due to bending but it does not account for the variation in the strain distribution caused by the local deformations of the tape and the Poisson's effect.

In this work, we used structural finite element analysis (FEA) to investigate the mechanical strain generated in the REBCO coated conductors during canted-cosθ (CCT) dipole winding with different winding angles. We investigated two different configurations: in configuration A (Fig. 1(a)), a flat tape lay in the mandrel's channel, while in configuration B (Fig. 2 (b)) the channel is filled with a tape pre-wound on a circular copper former (typical configuration of CORC® cable [13]). For this last structure, the strain accumulated during the tape's winding to

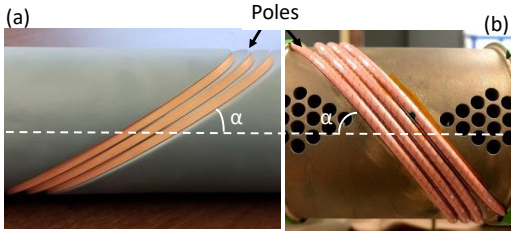

Fig. 1. CCT dipole winding using REBCO tapes as: (a) flat tape winding. (b) CORC cable. α is the tilt angle of the mandrel.

This work was supported by the Director, Office of Science, Office of Fusion Energy Sciences, of the US Department of Energy under Contract No. DEAC02-05CH11231. *(Corresponding author: Federica Pierro.)*

F. Pierro , Z. Zhao, C. M. Owen, C. Colcord and L. Chiesa are with the Mechanical Engineering Department, Tufts University, Medford, MA 02155 USA (email: {Federica.Pierro, Zijia.Zhao, Casey.Owen, Christopher.Colcord, Luisa.Chiesa}@tufts.edu).

H. Higley, X. Wang and S. O. Prestemon are with Lawrence Berkeley National Laboratory, Berkeley, CA 94720-8203 USA (e-mail: {hchigley,xrwang,soprestemeon}@lbl.gov).

Color versions of one or more of the figures in this paper are available online at http://ieeexplore.ieee.org.

Digital Object Identifier will be inserted here upon acceptance.

form the cable is also analyzed. Finite element results are validated experimentally both directly (measuring the strain) and indirectly (measuring the I_c degradation as a function of bending radius). Both experiments and simulations were performed on single tapes to highlight the effect of the mechanical strain on the I_c with minimal self-field effect caused by multi-tape configuration. The single tape configuration provided a simple and well-defined condition that allowed us to better understand the development of strain and its impact on the conductor critical current.

II. Finite Element Model

Static structural FEA using ANSYS® was used to study the strain distribution of a REBCO tape when wound and bent in the CCT configuration. The conductor was modelled with a 30 µm Hastelloy substrate and a 10 µm copper stabilizer. In the following sections, we describe the details of the FEA models, including geometry, mesh density, element types, boundary conditions and loading conditions for the two configurations. The effect of the winding rate is not included in this study (static analysis).

A. Boundary Conditions and Loading Conditions

Modelling was performed for a single tape in two different configurations: 1) a flat tape wound on an elliptical former (configuration A) and 2) a straight tape helically wound on copper core and then bent to reproduce the bending diameter at the pole of the elliptical former (configuration B), which is the most critical one. The geometry of the two configurations prior loading is shown in Fig. 2 (a) and (b), together with the applied boundary conditions. In both cases, the conductor is bent with the REBCO layer facing the former. This is the favorable configuration for winding because the REBCO layer will experience compression (reversible I_c reduction over a wider strain range compared to tensile strain).

1) Flat tape (configuration A)

In this configuration (Fig. 2 (a)) the tape is flat and straight, with one edge fixed to the former. A uniform load of 2 N is applied on the opposite edge of the tape to maintain tension during winding. On the same edge, a displacement of 6.6 mm (winding pitch from [12]), along the width's direction of the tape is applied.

The former is modelled as an elliptical surface. The curvature of the ellipse is determined by the tilt angle α. Motion of the former is controlled by a pilot node (using a multi-point coupling constrain) placed in the middle of the former. Winding is generated by applying a rotation of 360° to the pilot node.

2) Helically wound tape (configuration B)

This model consists of two steps. In the first step, a straight tape is wound around a copper core (Fig. 2 (b)). Then, in step 2, the resulting geometry is bent to mimic the bending diameter at the pole of the ellipse in the CCT configuration. In order to simplify the computation, pure bending is applied to a small section of the cable (three pitches) up to a bending diameter of 12 mm

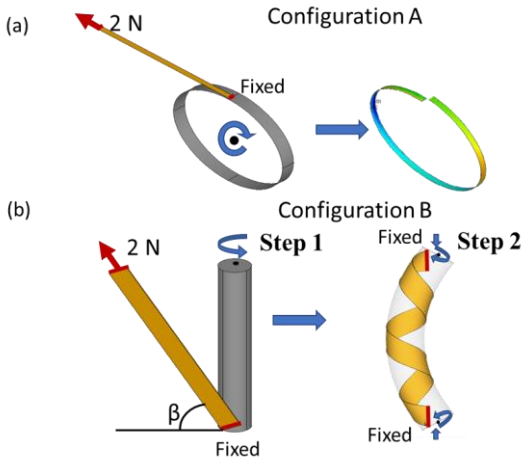

Fig. 2. Geometry and loading condition for: (a) configuration A and (b) configuration B. Configuration B is divided in two loading steps. For configuration A the longitudinal strain distribution after winding is also shown.

(which represent the bending diameter at the poles for a dipole with a mandrel's diameter of 70 mm and with a tilt angle α of 20°). One edge of the conductor is fixed to the copper core, while a tension of 2 N is applied on the other end of the tape. The tape is angled of β degrees (angle between the central axis of the tape and the normal to the central axis of the former). Two pilot nodes control the displacement of the two ends of the copper core as it undergoes a 360° rotation. In a second step, bending is generated by applying equal and opposite displacement and rotation to the pilot nodes at the ends of the cable.

B. Element Type, Mesh and Contact Relationships

The tape was modelled using SOLSH190, which is a solid-shell element with layer capability. Following the procedure described in [14] the tape was modelled as a uniform volume, while material properties of each layer are defined using shell section commands. The copper core (for the helically wound tape) was modelled using SOLID185.

The helical former representing the CCT mandrel (configuration A) was modelled as a rigid surface. In both configurations contact elements (TARGE170 and CONTA174) were used to describe the contact interaction between the copper core and the tape respectively. A friction coefficient of 0.2 was used between the surfaces. This value represents the typical friction coefficient between metals in liquid nitrogen [15].

A mesh study was conducted to identify the optimal number of elements. The tape was modelled with one element through its thickness, 20 elements across its width and an element size of 0.1 mm. The same element size was also chosen for the copper core and the CCT mandrel.

C. Material Properties

Material properties of the four main layers of REBCO tapes (copper, silver, REBCO/buffer and substrate), the copper core and the stainless-steel former are listed in Table I. The thermal strain from room temperature to 77 K is neglected in this study (negligible compared to bending strain) and material properties

at 77 K are assumed in the model. A bilinear isotropic model was used to describe the elasto-plastic behavior of the materials by defining: modulus of elasticity (E), yield strength (Y) and tangent modulus (T) for each material [16]-[24].

TABLE I
ISOTROPIC BILINEAR MATERIAL PROPERTIES AT 77 K [16]-[24]

Material	E (GPa)	Y (MPa)	T (GPa)
REBCO	150	--	--
Copper Stabilizer	81.5	340	8
Silver	90	235	22
Hastelloy	190	1250	7.5
Copper (core)	120	50	4.5
Stainless Steel	180	950	10

Note: Elastic modulus (E), offset yield stress (Y) and tangent modulus (T).

III. RESULTS AND DISCUSSIONS

For configuration A, the longitudinal strain along the tape length and across its width are presented. A parametric study on the former diameter and tilt angle is also conducted to investigate the change of the maximum stress with the geometric parameters of the dipole. For configuration B, longitudinal strain distribution is shown after winding (step 1) and bending (step 2). A parametric study is also conducted on the copper core diameter and winding angle, as well as the friction coefficient between the tape and the core. Experimental results are also compared to the simulations as a way to validate the FEA models. Two methods of comparison were used: 1) direct comparison between the strain measured with strain gauges mounted on the conductor and strain distribution from the model (for configuration A) and 2) indirect comparison of the normalized critical current (for configuration B). For the models, the normalized critical current is calculated by combining the longitudinal strain in the conductor with experimental results at 77 K [25], following the procedure described in [26].

A. Configuration A

Fig. 3 illustrates the average longitudinal strain along the length of the conductor bent in the CCT configuration. The maximum strain (both tensile for the top surface and compressive for the REBCO layer) is experienced at the two poles of the ellipse (of the CCT mandrel). In Fig.3 the strain obtained from FEA is compared with experimental results obtained with strain gauges located on the top surface of the tape prior to winding. The strain gauges were mounted so that they would be positioned at the pole of two mandrels (both having a diameter of 70 mm and a tilt angle of 20° and 30°) after winding. Comparing results of the simulation with strain gauge readings it was observed that a higher strain was measured with the strain gauges (about 25%). This mismatch could be caused by the thickness of the epoxy between the strain gauge and the tape. Additionally, in the FEA a tension of 2 N was applied to numerically execute the winding, while experimentally the tape was wound by hand without measuring the tension applied. However, the FEA results agrees with the strain calculated analytically using equations in [12]. Additionally, the FEA results show that the longitudinal strain is not constant across the tape's width. A variation of about 33% was observed between minimum and maximum longitudinal strain.

A parametric study was conducted on the former diameter as well as the tilt angle (Fig. 4) focusing on the strain in the REBCO layer, which is the one driving a possible reduction of I_c. Higher strain was observed at small tilt angles for the same former diameter (-0.12% at 20° compared to -0.045% at 50°, for a former diameter 65 mm). The increase in strain is less severe for changes in the former diameter than changes in the tilt angles. However, we do not expect I_c reduction over a wide strain range compared to tensile strain (<0.14%).

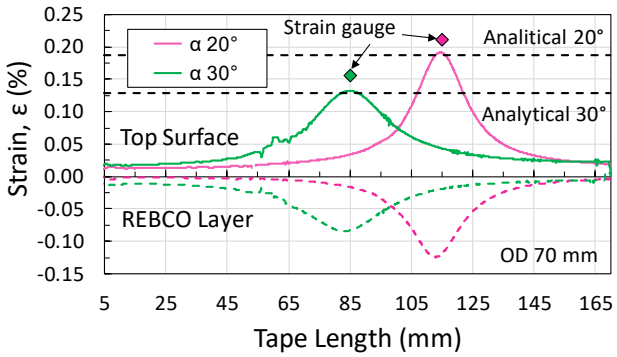

Fig. 3. Longitudinal strain along the tape's length. Tensile strain is experienced on the top surface of the tape (substrate's side), while compression is experienced in the REBCO layer. Results are averaged across the tape's width.

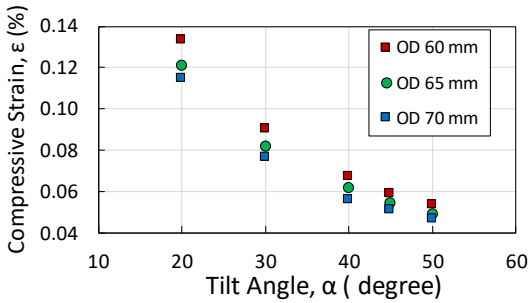

Fig. 4. Longitudinal strain in the REBCO layer (at the pole) as a function of former's diameters and tilt angles.

B. Configuration B

Fig. 5 shows the distribution of the longitudinal strain on the REBCO layer across the tape's width for a copper core diameter of 3 mm and a winding angle of 35°. It can be observed that the strain is not uniform across the tape's width but decreases in magnitude (REBCO layer is in compression) towards the edges of the tape. A parametric study investigating different core diameters as well as winding angles was conducted, and it showed that smaller cores as well as smaller winding angles result in higher compressive strain in the REBCO layer (Fig. 6).

Bending simulations were carried out for a copper core diameter of 3 mm and a winding angle of 35°. The effect of different friction coefficients was considered. The tape winding, as well as the subsequently bending was also replicated experimentally. Critical current of the conductor was first measured in the straight configuration. A 3 mm diameter 20 cm long annealed

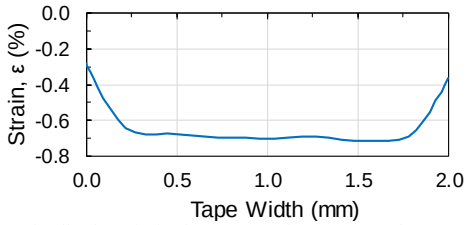

Fig. 5. Longitudinal strain in the REBCO layer across the tape's width for a core diameter of 30 mm and a winding angle of 35°.

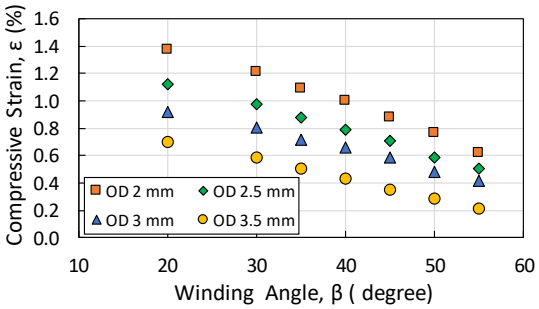

Fig. 6. Maximum (compressive) longitudinal strain in the REBCO layer after winding as a function of the copper core diameter and winding angle.

copper rod was used for the core. Winding of the tape was performed as shown in Fig. 7 (a). One end of the tape was fixed to the core while a tension was applied on the other end of the conductor with a 200 g weight. Rotation of the core was performed using a drill, which was rotated with respect to the horizontal plane of an angle β of 35°. After winding, both ends of the conductor were removed to eliminate potentially damaged end sections. Critical current was measured again after winding at 77 K and no degradation was observed. The wound single-tape was then bent around circular formers of the following diameters (Fig. 7 (b)): 100 mm, 50 mm, 32 mm and 20 mm. The critical current was measured after every bending step to determine the reduction of the I_c in the conductor.

The experimental results were compared to the critical current results evaluated numerically (estimated at each bending diameter for different friction coefficients).

In the FEA, the longitudinal strain was calculated at 40 Gaussian integration points across the tape's width and the normalized I_c was calculated at 20 different locations along the length of the tape to take in consideration the fact that the strain is not uniform along the length of the tape as it experiences tension and compression depending on its position with respect to the core. The minimum normalized I_c obtained was then defined as the one of the conductor. In Fig.8 the normalized I_c (estimated from the strain results of the model and normalized to the

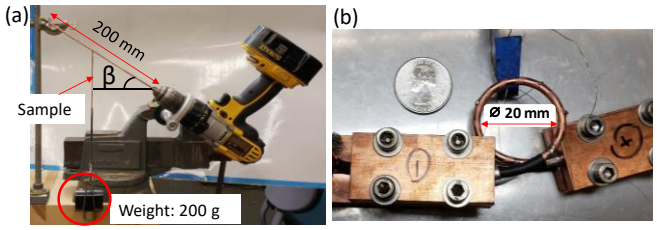

Fig. 7. Winding and bending technique for experimental validation.

current of the tape after winding, I_{co}) are plotted as a function of the bending diameter and compared with the experimental results. The FEA results show that an increase in friction between tape and the core results in a larger degradation (I_c/I_{co} is 75% at 30 mm bending diameter with μ=0.5). The numerical results with μ=0.2 agree well with the experimental results up to a bending diameter of 30 mm even if a smaller I_c degradation was observed at smaller bending diameter (~5%). Experimentally, this degradation was more severe (up to 15%). The difference could be caused by the difference in coefficient of friction between the model and the real-life situation. Depending on the tension during winding, the tape might be tighter on the core, therefore sliding less easily and experiencing a higher friction.

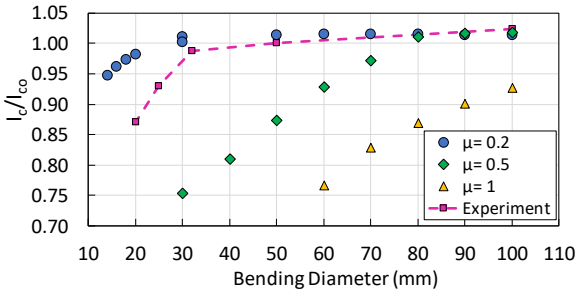

Fig. 8. I_c/I_{co} as a function of the bending diameter and friction coefficients. FEA results are compared with experimental data.

IV. Conclusion

Structural finite element was used to investigate the strain distribution in REBCO coated conductors due bending in a canted-cosθ dipole configuration using two different configurations: a flat tape and a helically wound tape. A parametric study was conducted on the former diameters and winding (for the helical winding) and tilting angles (for the flat tape configuration), suggesting that smaller former as well as smaller angles, results in higher strain accumulations. FEA results were compared with experimental findings. For configuration A, the strain measured with the strain gauges was higher (25%) than the FEA solution, which could be due to the thickness of the epoxy and the winding tension. FEA results match analytical calculations. For small tilt angles, we expect negligible I_c degradation to occur. For configuration B, experimental and numerical results are in good agreement up to a bending diameter of 30 mm. For smaller bending diameter the current degradation is higher in the tested sample, potentially due to a higher friction between the core and the tape. In this configuration, a degradation higher than 15% is expected for small bending diameters (which translate to small tilt angle).

We can conclude that configuration A appears to have smaller degradation compared to configuration B. More work will be necessary to better elucidate the dependence between mandrel's friction coefficient and the tape's architecture (thicker substrate and copper stabilizer). To extrapolate the behavior of an entire cable from the one of a single tape, the bending behavior of a stack of tape for configuration A and a multi-layer cable for configuration B will be modeled and evaluated. The magnetic field generated in both configurations will be also investigated.

REFERENCES

[1] L. Rossi et al., "The EuCARD-2 future magnets European collaboration for accelerator quality HTS magnets", *IEEE Trans. Appl. Supercond*., vol. 25, no. 3, June 2015, Art. no. 4001007

[2] A. Godeke, et al., "Limits of NbTi and Nb_3Sn, and Development of W&R Bi–2212 High Field Accelerator Magnets", *IEEE Trans. Appl. Supercond*., vol. 17, no. 2, pp. 1149-1152, June 2007.

[3] C. Lorin et al., "Cos-θ design of dipole inserts made of REBCO-Roebel or BSCCO-Rutherford cables", *IEEE Trans. Appl. Supercond*., vol. 25, no. 3, June 2015, Art. no. 4000305

[4] A. Godeke et al., "Bi-2212 canted-cosine-theta coils for high-field accelerator magnets", *IEEE Trans. Appl. Supercond.*, vol. 25, no 3, June 2015, Art. no. 4002404

[5] S. Caspi, et al., "Design of an 18-T canted cosine–theta superconducting dipole magnet", *IEEE Trans. Appl. Supercond.* vol. 25, no 3, June 2015 Art. no. 4000205

[6] X. Wang et al., "A viable dipole magnet concept with REBCO CORC® wires and further development needs for high-field magnet applications *Supercond. Sci. Technol.*, vol. 31, no. 4, March 2018, Art. no. 045007

[7] K. Koyanagi et al., "Development of saddle-shaped coils for accelerator magnets wound with YBCO-coated conductors", *IEEE Trans. Appl. Supercond.* vol. 25, no 3, June 2015, Art. no. 4003104

[8] LG. Fajardo et al., "Designs and Prospects of Bi-2212 Canted-Cosine-Theta Magnets to Increase the Magnetic Field of Accelerator Dipoles Beyond 15 T", *IEEE Trans. Appl. Supercond.* vol. 28, no .4 June 2018, Art. no. 4008305

[9] G. De Marzi et al., "Bending tests of HTS cable-in-conduit conductors for high-field magnet applications", *IEEE Trans. Appl. Supercond.* vol. 26, no. 4, June 2016, Art. no. 4801607

[10] VA. Anvar et al., "Bending of CORC® cables and wires: finite element parametric study and experimental validation", *Supercond. Sci. Technol.*, vol. 31, no.11, June 2018 Art. no. 115006

[11] M. Takayasu et al., "Analytical investigation in bending characteristic of twisted stacked-tape cable conductor", *IOP Conference Series: Materials Science and Engineering*, vol. 102, no. 1. IOP Publishing, 2015, Art. no. 012023

[12] X. Wang et al. "Strain Distribution in REBCO-Coated Conductors Bent with the Constant-Perimeter Geometry" *IEEE Trans. Appl. Supercond., vol*. 27 no. 8, December 2017, Art. no. 6604010

[13] D. van der Laan et al., "YBa2Cu3O7− δ coated conductor cabling for low ac-loss and high-field magnet applications", *Supercond. Sci. Technol, vol*. 22 no. 6, April 2009, Art. no. 065013.

[14] NC. Allen et al., "Structural modeling of HTS tapes and cables", *Cryogenics*, vol. 80, no. 3, pp. 405-418, December 2016.

[15] SY. Hong et al., "Experimental evaluation of friction coefficient and liquid nitrogen lubrication effect in cryogenic machining" *Mach. Sci. and Tech.*, vol. 6, no. 2, August 2006, Art. no. 120005958

[16] K. Goretta et al., "Mechanical properties of high-temperature superconducting wires", *Proc. of 4th World Congress on Supercond*, NASA Conference Publication, pp. 633-638, June 1994

[17] AS. Raynes et al, "Fracture toughness of YBa2Cu3O6+δ single crystals: Anisotropy and twinning effects", *J. Appl. Phys.* vol 70 no 10, August 1998, Art. no. 5254

[18] H. Ledbetter H et al, "Monocrystal elastic constants of orthotropic YBCO: An estimate", *J. Mater. Res.*, vol 6, pp 2253–5, 1991

[19] Ar. Nisay et al, "Mechanical and electro-mechanical analysis in differently stabilized GdBCO coated conductor tapes with stainless steel substrate", *Supercond. and Cryog*, vol. 15, no. 2, June 2013

[20] JW. Ekin, "Experimental techniques for low-temperature measurements" *Oxford Univ. Press*, October 2006.

[21] RP. Reed et al, "Materials at low temperatures", *American Society for Metals*, 1983

[22] Matweb – Material Property Data Website: Hastelloy® C-276 alloy [On- line]. Available: http://matweb.com/search/DataSheet.aspx?MatGUID=4361b68268934746ad70542944cdd8cf, Accessed on December 11, 2018.

[23] Matweb—Material Property Data Website: Oxygen-free high conductivity Copper, Soft, UNS C10200. [On- line]. Available: http://www.matweb.com/search/DataSheet.aspx?MatGUID=a629b7c5643b44bfb25b9bba7f8140ab, Accessed on December 11, 2018.

[24] Matweb – Material Property Data Website: Stainless Steel Type 304, 20% Cold Rolled. [On- line]. Available: http://www.matweb.com/search/DataSheet.aspx?MatGUID=1462ed9ca5334a75b52e748b3f3195e5, Accessed on December 11, 2018.

[25] Pierro F *et al*. "Critical Current Measurements of REBCO Tapes as a Function of Strain, Magnetic Field (12-15 T) and Temperature (4.2-40 K)", *IEEE Trans. Appl. Supercond*., Submitted for publication

[26] M. Takayasu et al., "HTS twisted stacked-tape cable conductor." Supercond. Sci. Technol., vol. 25, no. 1, December 2011, Art. no. 014011.